Site-specific electronic configurations of Fe 3 d states by energy loss by channeled electrons

Kazuyoshi Tatsumi, Shunsuke Muto, Ikuo Nishida, and Ján Rusz

Citation: Applied Physics Letters **96**, 201911 (2010); doi: 10.1063/1.3429593
View online: http://dx.doi.org/10.1063/1.3429593
View Table of Contents: http://scitation.aip.org/content/aip/journal/apl/96/20?ver=pdfcov
Published by the AIP Publishing

Site-specific electronic configurations of Fe 3*d* states by energy loss by channeled electrons

Kazuyoshi Tatsumi,[1,a)] Shunsuke Muto,[1] Ikuo Nishida,[1] and Ján Rusz[2]
[1]*Department of Materials, Physics, and Energy Engineering, Nagoya University, Chikusa, Nagoya 464-8603, Japan*
[2]*Department of Physics and Astronomy, Uppsala University, Box 516, SE-75120 Uppsala, Sweden*

(Received 24 March 2010; accepted 22 April 2010; published online 21 May 2010)

Site-specific configurations of Fe 3*d* electrons in a spinel ferrite were investigated by electron energy loss spectroscopy under electron channeling conditions. Site-specific spectra were extracted by applying a multivariate curve resolution (MCR) technique to the data set. An electronic difference in the Fe sites caused by ligand field splitting of trivalent Fe was probed. This demonstrated the promise of site-specific valence and spin state analysis in spintronics applications of spinel ferrites. © *2010 American Institute of Physics*. [doi:10.1063/1.3429593]

Electron channeling along specific lattice planes or atomic columns in crystalline materials is a well-known phenomenon that has been utilized for atomic site-selective analysis in energy dispersive x-ray spectroscopy and electron energy loss spectroscopy (EELS). The former can quantify the elemental concentration of an impurity at a specific site, known as atom-location by channeling-enhanced microanalysis. EELS analysis utilizing the channeling effect was first reported by Taftø *et al.*[1] Two kinds of channeling-enhanced Fe $L_{2,3}$ EEL near-edge structures (ELNES) in a chromite spinel well revealed chemical shifts due to their site-specific Fe valence states, i.e., Fe^{2+} at the tetrahedrally coordinated site and Fe^{3+} at the octahedrally coordinated site. One obstacle preventing more quantitative site-selective EELS analysis is the low signal-to-noise ratio under channeling conditions, which occurs because the EELS entrance aperture must be placed off-axis[1] to enhance the localization of the propagating electron wave. Another obstacle is that the experimentally obtained spectrum is inevitably a mixed spectrum from both sites, rather than an isolated pure component. In this letter, we report a site-specific electronic structure difference of Fe, caused essentially by ligand field splitting and detected by site-specific ELNES and associated theoretical calculations. The present method of analysis will help clarify the configurations of transition metal 3*d* electrons, which have been essential but still debatable, especially in spintronics applications of spinel ferrites.

A spinel ferrite, $NiFe_2O_4$, was studied. There are two nonequivalent crystallographic cation sites, tetrahedrally coordinated and octahedrally coordinated, as in the chromite spinel of Taftø *et al.* The octahedral sites are on the {400} planes with the anion sites, and the tetrahedral sites are located between the planes. Most of the Ni atoms occupy the octahedral sites, with $\delta = \sim 0.01$ in the formula $(Fe_{1-\delta}Ni_{\delta})^{\text{tet. site}}(Fe_{1+\delta}Ni_{1-\delta})^{\text{oct. site}}O_4$.[2] At the 400 excitation error $S_{400} < 0$ with *n*00 systematic reflections, the fast electron propagates along the (400) planes of the octahedral sites in the crystal, according to the many-beam dynamical calculation, as shown later. The present EELS entrance aperture was located off-axis along the 400 Kikuchi line, which allowed the same boundary conditions to apply to incoming and outgoing waves. We improved the resulting decreased S/N ratios by our recently developed on-line script, which accumulates EELS signals while correcting for the energy drift caused by external stray fields.[3] We then developed a on-line controlled beam rocking system in combination with the drift correction script to perform an automatic measurement of a series of ELNES, consecutively varying the excitation error around a specific Bragg condition. Fe and Ni $L_{2,3}$ ELNES with improved S/N ratios were collected with at 15 different incident beam orientations. The total exposure time for a single spectrum was 5 s × 20 and a collection semiangle was 7.5 mrad. The energy dispersion was 0.05 eV/channel and the energy resolution was about 1.0 eV, as estimated from the full width at half maximum of the zero-loss peak.

The acquired 15 spectra and the diffraction patterns (DPs) corresponding to the first (no. 1) and last (no. 15) beam orientations are shown in Fig. 1. The magnitudes of S_{400} at nos. 1 and 15 were estimated from the DPs to be -0.05 nm^{-1} and 0.04 nm^{-1}, respectively. The series of Fe spectra exhibited a gradual change in the shoulder structure at 709 eV, which was particularly distinct in the spectra numbered from nos. 1 to 8 collected at $S_{400} < 0$. Because most Ni atoms occupy the octahedral site, no significant difference was found in the profiles of the Ni spectra, except that their relative intensities increased at $S_{400} < 0$ due to preferential site selectivity.

The obtained spectra in Fig. 1 should be mixture of spectra from pure site-specific spectral components, whose weights varied with beam orientation. Given *n* energy bins, *l* site-specific pure components, and *m* mixed spectra, the experimental data set of the mixed spectra can be represented by a matrix $\mathbf{D}(m \times n)$, which can be regarded as a linear combination of the pure spectra,

$$\mathbf{D} = \mathbf{W}\mathbf{S}^{\mathbf{T}} + \mathbf{E}, \tag{1}$$

where an $n \times l$ matrix $\mathbf{S}$ represents the set of the pure spectra, an $m \times l$ matrix $\mathbf{W}$ represents their weights, and $\mathbf{E}$ denotes the residual components not explained by *l* components, such as statistical noise. *n*, *m*, and *l* were 2220, 15, and 2, respectively. We extracted $\mathbf{S}$ and $\mathbf{W}$ from $\mathbf{D}$ by a multivariate curve resolution (MCR) technique which has been applied in Refs. 4 and 5.

a)Electronic mail: k-tatsumi@nucl.nagoya-u.ac.jp.

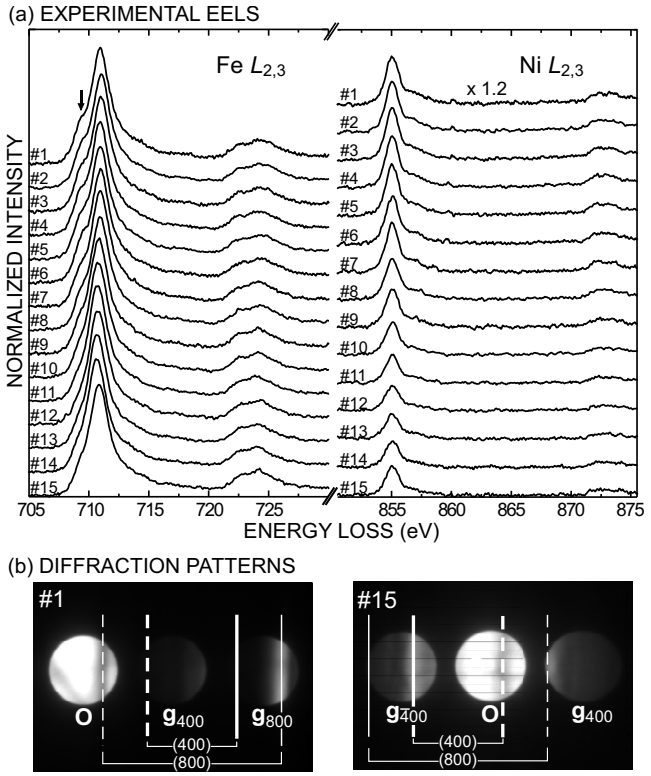

FIG. 1. (a) Fe and Ni $L_{2,3}$ ELNES collected under 15 different diffraction conditions. The spectra are normalized so that the peak maxima of Fe ELNES exhibit the same height. The total exposure time per spectrum was 5 s × 20. The energy resolution was 1.0 eV. (b) The DPs corresponding to nos. 1 and 15 spectra in (a). The thick (thin) vertical lines denote the positions of the set of 400 (800) Kikuchi lines. We set a beam convergence semiangle of 4.6 mrad, a collection semiangle of 7.5 mrad, and an EELS entrance aperture off-axis shift of 1.5 $|\mathbf{g}_{400}|$.

We defined the site-selectivity F_t, of a mixed spectrum obtained at a diffraction condition, using the corresponding elements of **W**, by $F_t = W_{tet}/(W_{tet}+W_{oct})$, where W_{tet} and W_{oct} are the weights of the tetrahedral and octahedral site spectral components, respectively. We theoretically calculated F_t for the Fe $L_{2,3}$ shell,[6] assuming the nominal atomic site occupancy of $(Fe_I)^{tet.\ site}(Fe_INi_I)^{oct.\ site}O_4$, as a function of the incident beam orientation based on Schattschneider's formulation,[7] incorporating both elastic and inelastic dynamical scattering of many beams.[8,9] The number of incorporated beams was 18 to 24, depending on the diffraction conditions. As shown in Fig. 2, the theoretical F_t curve was consistent with the experimental one, confirming the validity of the present MCR results.

The site-specific pure spectra extracted from the matrix **S** were compared with theoretical spectra. These were calculated[6] by an *ab initio* configuration interaction (CI) method[10–13] using a basis set of Slater determinants composed of completely relativistic molecular orbitals, of Fe $2p$, $3d$, and O $2p$, which were obtained using FeO_6 and FeO_4 model clusters specific to the octahedral and tetrahedral sites. In order to take the effective Madelung potential into account, point charges were placed at external atomic sites. The experimental spectra were consistent with the theoretical spectra of Fe^{3+} in the corresponding specific clusters, as shown in Fig. 3. The main peak B_{oct} shifted to an energy 0.4 eV higher than the main experimental peak B_{tet}, in good agreement with the 0.5 eV chemical shift in the calculation.

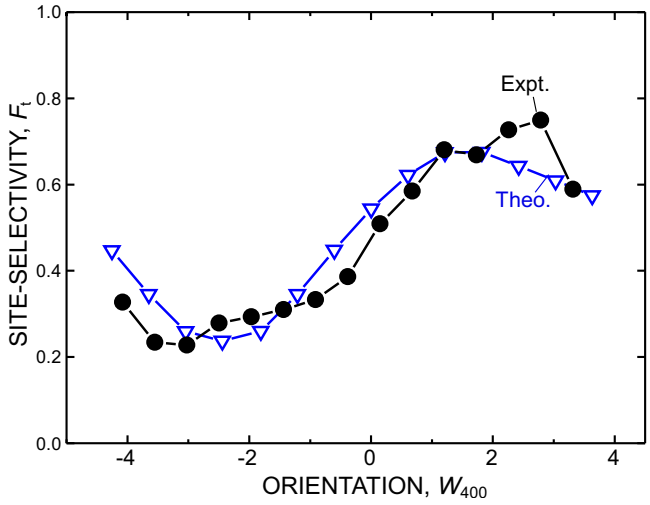

FIG. 2. (Color online) Comparison between the theoretical and experimental site-selectivity, F_t with respect to the incident beam orientation, which is represented by a dimensionless parameter $W_{400}=S_{400}\xi_{400}$, where ξ_{400} is the extinction distance of the 400 beam. We set the same aperture conditions as in the experiment.

The subpeak A_{oct} was more intense than A_{tet} in both the experiment and the calculation.

Since the *ab initio* CI reproduced the experimental spectral features associated with the two sites quite well, we can

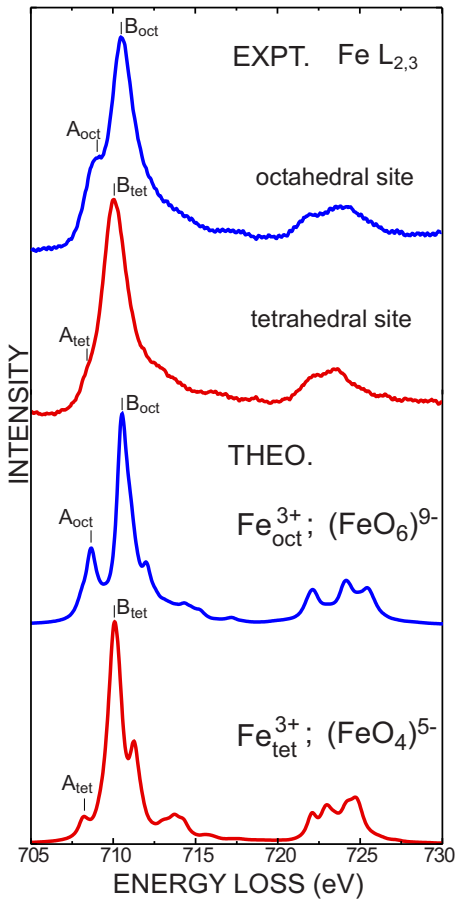

FIG. 3. (Color online) Comparison between theoretical and experimental site-specific Fe $L_{2,3}$ ELNES. The energy resolution in the experimental spectra was 1.0 eV. The theoretical spectra were obtained by convoluting a 0.6 eV Lorenz function with the discrete transition probabilities so as to show the fine structures clearly.

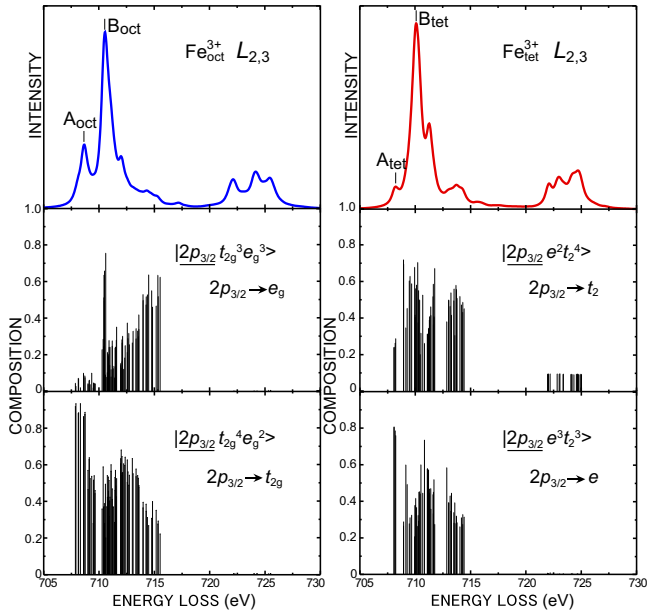

FIG. 4. (Color online) Configuration analysis of many-electron wave functions corresponding to the final states of peaks A and B in the Fe L_3 edge. Because the basis set of the Slater determinants $\{\phi_p\}$ are orthonormal, using an eigenvector $\{C_p\}$, an electron configuration Ξ's composition is simply given by $\Sigma_{p\in\Xi}|C_p|^2$.

further discuss the site-specific electronic structures using the calculation results. Because the Fe valence states in the two theoretical spectra were both trivalent, the above differences between the site-specific spectra should be ascribed to electronic configurations other than the valence state. The one-electron energy levels of Fe $3d$ states were split into two groups in the molecular orbital calculation. Assuming the O_h and T_d symmetry in the ligand fields for Fe_{oct} and Fe_{tet}, we denote the lower and higher energy levels of Fe_{oct} as t_{2g} and e_g, and those of Fe_{tet} as e and t_2 using the nonrelativistic irreducible representation labels of the symmetry groups for simplicity. The calculated many-electron ground states were composed of three t_{2g} and two e_g levels, $|t_{2g}^3 e_g^2\rangle$ for Fe_{oct}, and two e and three t_2 levels, $|e^2 t_2^3\rangle$ for Fe_{tet}. These configurations indicate high-spin ground states, because the corresponding nonrelativistic $3d$ electron levels have an energy E in the order of $E(t_{2g}^{\uparrow})<E(e_g^{\uparrow})<E(t_{2g}^{\downarrow})<E(t_{2g}^{\downarrow})$ and $E(e^{\uparrow})<E(t_2^{\uparrow})<E(e^{\downarrow})<E(t_2^{\downarrow})$ and stable electron occupations are $|t_{2g}^{\uparrow 3} e_g^{\uparrow 2}\rangle$ and $|e^{\uparrow 2} t_2^{\uparrow 3}\rangle$, as the energy splitting of the spin-orbit coupling is nearly one-tenth of the energy-splitting of the spin-polarization and ligand field. The peaks A and B in the L_3 edge structures mainly correspond to two kinds of excitation configurations containing a $2p_{3/2}$ hole and an extra $3d$ electron. These are represented as $|\underline{2p_{3/2}} t_{2g}^4 e_g^2\rangle$ and $|\underline{2p_{3/2}} t_{2g}^3 e_g^3\rangle$ for Fe_{oct}, and $|\underline{2p_{3/2}} e^3 t_2^3\rangle$ and $|\underline{2p_{3/2}} e^2 t_2^4\rangle$ for Fe_{tet}, where the underlines indicate that the core level contains a hole. The compositions of these four configurations in the theoretical many-electron energy levels are plotted in Fig. 4, in conjunction with the theoretical Fe $L_{2,3}$ spectra. In the Fe_{oct} spectrum, $|\underline{2p_{3/2}} t_{2g}^4 e_g^2\rangle$ ($|\underline{2p_{3/2}} t_{2g}^3 e_g^3\rangle$) had a larger fraction for A_{oct} (B_{oct}), while the $|\underline{2p_{3/2}} e^3 t_2^3\rangle$ ($|\underline{2p_{3/2}} e^2 t_2^4\rangle$) fraction was relatively larger for A_{tet} (B_{tet}). Therefore, peaks A_{oct} and A_{tet} were associated with the one-electron lower energy levels t_{2g} and e, respectively, which contain three and two holes at the ground states, respectively. This qualitatively explains the relative intensity difference of peak A.

In summary, improving the method originated by Taftø *et al.*[1] in a more quantitative manner, we have observed in a site-selective manner an electronic structure difference in Fe atoms, which was caused not by different valence, but by ligand field splitting. We have identified the $3d$ electronic configurations as high-spin trivalent states by comparing the experimental site-specific ELNES with first principles calculations.

The site-specific $3d$ electronic configurations, especially the valence states and spin states in some transition metal oxides, including spinel ferrites in spintronics applications, have been controversial, and there have been inconsistencies among some of the published studies.[14–16] The present method will become an important analytical technique, because the experiment directly provides site-specific electronic spectra, and the *ab initio* calculations provide information on the excited states and the ground state electronic structures.

This work was supported in part by a Grant-in-Aid for Scientific Research of MEXT Japan (Priority Area #474 "Atomic Scale Modification"), JSPS (Wakate B: 21760516), and the MST Foundation.

[1] J. Taftø and O. L. Krivanek, Phys. Rev. Lett. **48**, 560 (1982).
[2] M. A. F. Ramalho, L. Gama, S. G. Antonio, C. O. Paiva-Santos, E. J. Miola, R. H. G. A. Kiminami, and A. C. F. M. Costa, J. Mater. Sci. **42**, 3603 (2007).
[3] Y. Sasano and S. Muto, J. Electron Microsc. **57**, 149 (2008).
[4] Y. Yamamoto, K. Tatsumi, and S. Muto, Mater. Trans. **48**, 2590 (2007).
[5] K. Tatsumi and S. Muto, J. Phys.: Condens. Matter **21**, 104213 (2009).
[6] In both of the calculations, other transitions than the electric dipole transition were neglected since we found their probabilities insignificant.
[7] P. Schattschneider, B. Jouffrey, and M. Nelhiebel, Phys. Rev. B **54**, 3861 (1996).
[8] P. Schattschneider, M. Nelhiebel, M. Schenner, W. Grogger, and F. Hofer, J. Microsc. **183**, 18 (1996).
[9] J. Rusz, S. Rubino, and P. Schattschneider, Phys. Rev. B **75**, 214425 (2007).
[10] H. Ikeno, F. M. F. de Groot, E. Stavitski, and I. Tanaka, J. Phys.: Condens. Matter **21**, 104208 (2009).
[11] H. Ikeno, T. Mizoguchi, Y. Koyama, Y. Kumagai, and I. Tanaka, Ultramicroscopy **106**, 970 (2006).
[12] H. Ikeno, I. Tanka, Y. Koyama, T. Mizoguchi, and K. Ogasawara, Phys. Rev. B **72**, 075123 (2005).
[13] K. Ogasawara, T. Iwata, Y. Koyama, T. Ishii, I. Tanaka, and H. Adachi, Phys. Rev. B **64**, 115413 (2001).
[14] H. J. Lee, G. Kim, J.-S. Kang, C. L. Zhang, S.-W. Cheong, J. H. Shim, H. Lee, J.-Y. Kim, B. H. Kim, and B. I. Min, J. Phys.: Condens. Matter **20**, 295203 (2008).
[15] J. Takaobushi, M. Ishikawa, S. Ueda, E. Ikenaga, J.-J. Kim, M. Kobata, Y. Takeda, Y. Saitoh, M. Yabashi, Y. Nishino, D. Miwa, K. Tamasaku, T. Ishikawa, I. Satoh, H. Tanaka, K. Kobayashi, and T. Kawai, Phys. Rev. B **76**, 205108 (2007).
[16] J.-S. Kang, G. Kim, H. J. Lee, D. H. Kim, H. S. Kim, J. H. Shim, S. Lee, H. Lee, J.-Y. Kim, B. H. Kim, and B. I. Min, Phys. Rev. B **77**, 035121 (2008).